Eur Biophys J (2004) 33: 469–476
DOI 10.1007/s00249-004-0397-0

ARTICLE

Hitoshi Suda · Naoya Sasaki · Yuji C. Sasaki
Kenya Goto

Force generation by recombinant myosin heads trapped between two functionalized surfaces

Received: 19 March 2003 / Revised: 20 June 2003 / Accepted: 16 July 2003 / Published online: 13 March 2004

Abstract Fluorescence resonance energy transfer measurements have revealed that the lever-arm domain of myosin swings when it hydrolyzes Mg-ATP. It is generally accepted that this swing of the lever arm of myosin is the molecular basis of force generation. On the other hand, the possibility that the force might be generated at the interface between actin and myosin cannot be ignored. However, there is a third possibility, namely, that myosin itself generates force without actin. Thus, using recombinant subfragment 1 molecules of *Dictyostelium* myosin II that were trapped between two functionalized surfaces of a surface-force apparatus, we determined whether myosin itself could actually generate force. Here, we report that, despite the absence of actin, myosin heads themselves have a capacity to generate a force (at least ~0.2 pN/molecule) that is coupled to the structural changes. Although the role of actin should not be neglected because muscle physiologically shortens as a result of the interaction between actin and myosin, in this work the focus is on the question of whether the catalytic domain of myosin has the capacity to generate force.

H. Suda (✉)
Department of Biological Science and Technology,
Tokai University, 317 Nishino,
Numazu, 410-0321 Shizuoka, Japan
E-mail: suda@fb.u-tokai.ac.jp

N. Sasaki
Center for Interdisciplinary Research,
Tohoku University, Aoba,
Aramaki, Aobaku, Sendai,
980-8579 Miyagi, Japan

Y. C. Sasaki
Japan Synchrotron Radiation Research Institute,
SPring-8, CREST/JST, Mikazuki,
679-5198 Hyogo, Japan

K. Goto
Department of Information and Communication Technology,
Tokai University, 317 Nishino, Numazu,
410-0321 Shizuoka, Japan

Keywords Force generation · Force measurement · Functionalized surface · Motor protein · Recombinant myosin

Introduction

The molecular motor myosin is generally understood to swing its long lever-arm domain upon hydrolyzing Mg-ATP bound to the catalytic domain (Huxley 1957, 1969; Irving et al. 1992; Wakabayashi et al. 1992; Rayment et al. 1993a, 1993b; Irving et al. 1995; Dominguez et al. 1998; Dobbie et al. 1998; Geeves and Holmes 1999). Using single muscle fibers, the swinging motion of myosin heads has been proved to produce a force with their structural changes (Irving et al. 1992, 1995; Dobbie et al. 1998). However, the possibility cannot be ignored that the force might be generated at the interface between actin and myosin and that the detected tilting motion of the lever-arm domain might be a mere deformation caused by the generated force. These possibilities imply that there is no causal relationship between the lever-arm motion and the force generation (Yanagida and Iwane 2000). On the other hand, dynamic structural changes (Suzuki et al. 1998; Shih et al. 2000) of myosin heads in solution have been measured by using fluorescence resonance energy transfer (FRET), where the force was not measured simultaneously. According to the lever-arm model (Rayment et al. 1993a; Finer et al. 1994; Baker et al. 1998), the force generation is usually interpreted to be due to a coupling of the interaction between the swinging lever-arm and the actin filament. Muscle physiologically shortens as a result of interaction between actin and myosin; therefore, the important role of actin should not be ignored. However, for the molecular basis of force generation in muscle contraction, there is a third interpretation, namely, that myosin itself generates force without actin. Concerning this third model, the following interpretation is possible: in muscle contraction, the generated

force by individual myosin molecules is probably transferred to actin filaments through the interface between actin and myosin, causing muscles to shorten. If this is the case, actin filament may be interpreted to play the following two important roles. One is a track-like function that restricts the movable direction one-dimensionally, and the other is an acceleration that is about 200 times higher than the turnover rate of ATP hydrolysis in myosin. To test our model using a surface force apparatus (SFA) (Lee and Belfort 1989; Suda et al. 1999; Jeppesen et al. 2001), we constructed recombinant myosin for a myosin subfragment-1 (S1) of *Dictyostelium* myosin II. As a result, the force could be first detected by capturing two termini of recombinant S1 molecules between two chemically functionalized silica surfaces. Here, using a new force detection method, we show that, despite the absence of actin, myosin heads themselves generate a force that is coupled to their structural changes. Our finding was first made possible because the extreme sensitivity of the present force-detection technique allows changes in force per molecule to be measured with an accuracy of ~0.01 pN.

Materials and methods

Construction of recombinant myosin subfragment-1

The S1 molecule was genetically modified so that a reactive cysteine residue was introduced into the myopathy loop located at the tip of the molecule. The *Dictyostelium* myosin II gene was modified to change D402 in the myopathy loop at the tip of the head to CR so that the surface loop contains the –RCR– sequence. It has been shown that the cysteine residue sandwiched with arginine residues has high reactivity toward the maleimide group (unpublished results). A histidine tag was also genetically fused to the NH_2 terminus of the regulatory light chain, which is located at the other end of the molecule opposite to the myopathy loop, to trap the molecule between two surfaces of SFA. The recombinant S1 was expressed in *Dictyostelium* cells and purified as described previously (Sasaki et al. 1998).

The introduction of the –RCR– sequence into the myopathy loop did not significantly affect the motor functions of myosin. These were determined by using the conventional in vitro motility assay for the gliding speed of actin filaments and the malachite green method for the P_i quantitative analysis as described previously (Itakura et al. 1993). In fact, the V_{max} and K_m values of actin-activated ATPase activities of the recombinant full-length myosin, including D402CR-S1, were 0.25 ± 0.05 s^{-1} (mean ± s.d., $n = 3$) and 0.04 ± 0.03 μM, respectively, whereas those of the wild-type myosin were 0.05 ± 0.05 s^{-1} and 0.50 ± 0.03 μM, respectively. Also, the basal ATPase rate of the recombinant S1 was 0.04 s^{-1}. The sliding velocity of the actin filament driven by the recombinant full-length myosin was 0.52 ± 0.25 μm s^{-1} (mean ± s.d., $n = 457$), whereas that of the wild-type myosin was 1.20 ± 0.25 μm s^{-1}.

Myofibrils

We prepared myofibrils from a rabbit glycerinated psoas muscle fiber (diameter ~1 mm) that was immersed in 50% glycerol including 5 mM EGTA for at least one month in a freezer at −20 °C. These were used to estimate the damage effects of UV radiation and the amount of ATP released from a caged ATP solution by UV irradiation. The shortening speeds of the myofibrils were analyzed on a computer through an image capturing board connected to an S-VHS videocassette recorder. Experiments were carried out at 25 °C.

Preparation of silica thin films, chemical modification, and density of recombinant S1

In order to capture the recombinant S1 molecules between two smooth surfaces, silica (SiO_2) was deposited 100 nm thick onto mica surfaces by using an electron cyclotron radiation sputtering instrument (3400UD, NTT AFTY Corp., Japan). A thin film of SiO_2 was made on a 1–3 μm thick mica sheet mounted on a silica cylindrical lens (Fig. 1). The root-mean-square roughness of the silica-deposited surface was shown to be 0.55 nm by an AFM (SPM-9500J, Shimadzu, Japan) and scanning of a 1 μm×1 μm area with a pyramidal Si_3N_4 tip and a non-contact mode. The contact angle of a water droplet at the surface was $7.4 \pm 2.1°$ (mean ± s.d., $n = 5$).

The outermost surface of one side was finally exposed by nitrilotriacetic acid (NTA), and the other surface was exposed by maleimide groups. The NTA and maleimide exposed on silica surfaces were prepared as follows by successive heterocoupling processes (Sasaki et al. 2000). First, the surface of the deposited silica substrate on mica was treated with a 0.1% dilute solution of the aminosilane 3-(2-aminoethylaminopropyl)trimethoxysilane. After that, unbound reagents on the surface were gently removed by ultrasonic cleaning. Then, to cover the outermost surface with the thiol groups (–SH), the amino-coated surface was reacted with a 10 mM WSC cross-linker [1-ethyl-3-(3-dimethylaminopropyl)carbodiimide hydrochloride] including 2 mM sodium mercaptoacetate. After rinsing the surface with twice-distilled dust-free water, this thiol-covered surface was finally reacted with 10 mM maleimido-C3-NTA ligand (Dojindo, Japan). The Ni^{2+}-bound NTA surface was made by reacting with 50 mM $NiCl_2$ at room temperature for 10 min. On the other hand, the maleimide-exposed surface was made by reacting 5 mM sulfo-HMCS [*N*-(8-maleimidocapryloxy)sulfosuccinimide and sodium salt] with the amino-coated surface.

A 30-μL droplet of the recombinant S1 solution [~1 mg mL^{-1}, 50 mM NaCl, 10 mM MOPS (pH 7.4)] was put on the Ni^{2+}-NTA-covered surface and reacted for ~30 min at 25 °C. The adsorption reaction of the recombinant S1 was stopped by rinsing sufficiently with the dust-free solution. This disk was immediately set on the lower double cantilever and immersed shortly thereafter in a caged ATP solution [1 mM caged ATP (P^3-[1-(2-nitrophenyl)ethyl]adenosine 5′-triphosphate, trisodium salt; Dojindo, Japan], 15 mM KCl, 4 mM $MgCl_2$, [20 mM DTT (dithiothreitol), 40 mM MOPS (pH 7.0)], where DTT was independently added after capturing two termini of S1. As control experiments, we used the caged ADP solution (P^2-[1-(2-nitrophenyl)ethyl]adenosine 5′-diphosphate, disodium salt; Dojindo) that contained 1 mM caged ADP instead of caged ATP.

The area occupied by the recombinant S1 on the Ni^{2+}-NTA-covered surface was obtained by using a quartz crystal microbalance (oscillation frequency of 6 MHz, 16.3 ng Hz^{-1}; Hokuto Denko, Japan). The SiO_2 deposition and the chemical modification on an Au substrate were carried out at the same conditions as the SFA experiment. We controlled the temperature of the Au electrode to within ±0.1 °C because this detector is extremely sensitive to temperature change.

Evaluation of elasticity, density, and contact area by using the Hertz theory

The SFA (Lee and Belfort 1989; Suda et al. 1999; Jeppesen et al. 2001) was employed to detect the force generation of the recombinant S1 trapped at two points, as described above. The distance between the two surfaces was numerically analyzed with subnanometer accuracy (~0.1 nm) by using multiple interferome-

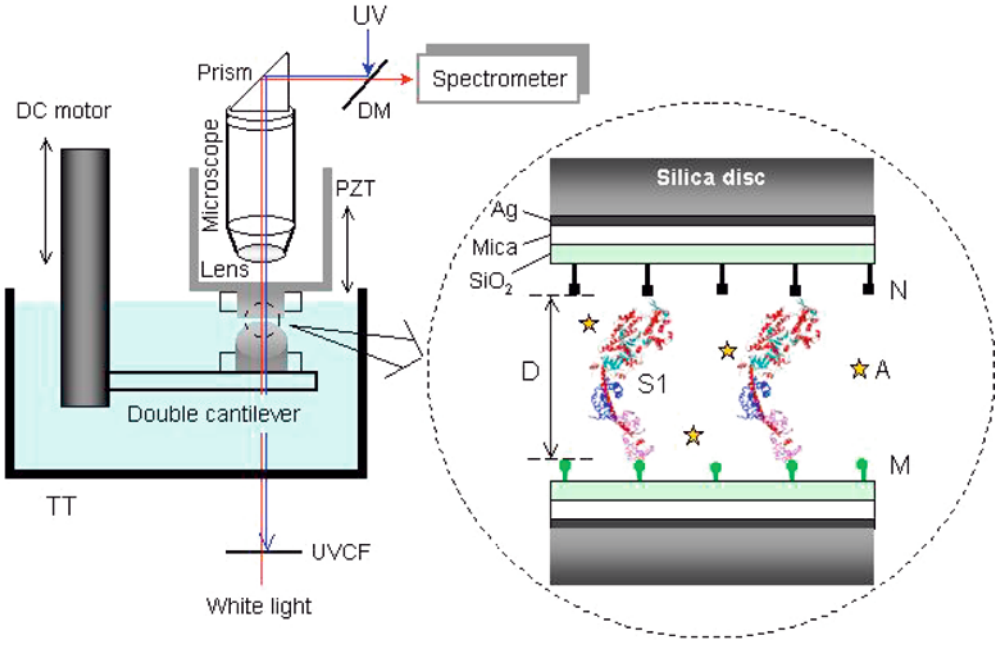

Fig. 1 Schematic diagram of force measurement of trapped recombinant S1 in the surface force apparatus (SFA). The recombinant S1 molecules are captured in a confined space between two chemically modified SiO_2 surfaces mounted on silica discs. The illustrated recombinant S1 is based on the atomic model in Rayment et al. (1993b). One of the two surfaces is exposed by maleimide groups (*M*, *small green circle*); the other is covered by Ni^{2+}-NTA (*N*, *small filled black square*). *D* denotes the distance between the maleimide- and Ni^{2+}-NTA-coated surfaces, and $D=0$ indicates the contact position of their surfaces. ATP was released by the irradiation of UV light on the local contact area through a dichroic mirror (*DM*) between a mirrored prism and a spectrometer, where a Teflon tank (*TT*) is filled by a solution (*light blue*) containing caged ATP (*gold star*, *A*). *UVCF*, UV-cut filter (<495 nm); *PZT*, piezoelectric tube. The scale is arbitrary

ters and the matrix method (Mangipudi 1995). The maleimide-covered surface attached to a PZT in the SFA was carefully approached to the recombinant S1-monolayer surface formed on the Ni^{2+}-NTA-covered surface of the opposite disk until the two surfaces made contact. Finally, an SH group of inserted cysteine residue covalently bound with a maleimide group, and the recombinant S1 molecules were captured between the confined space of two functionalized surfaces in the SFA. The contact area and the number of trapped recombinant S1 molecules between two surfaces were evaluated by Hertz's elastic theory as previously described (Suda et al. 1999).

Hertz (1881) studied the size and shape of the zone of contact between two smooth elastic bodies. In the SFA, the crossed cylinder configuration may be approximately replaced by spherical and flat surfaces, which is well known as the Derjaguin approximation (Israelachvili 1992, see section 10.5). For the sphere of radius R and planar surface pressed together under a load ΔF, the radius r_0 of the circle of contact area is given by $r_0^3=(3/4)\pi(K_{mica+KS1})R\Delta F$, where K_{mica} and K_{S1} are the elastic constants of each material; that is $K_{mica}=(1-\nu_{mica}^2)/(\pi E_{mica})$ and $K_{S1}=(1-\nu_{S1}^2)/(\pi E_{S1})$, where ν is the Poisson ratio and E the Young's modulus of each material. As a result of local compression near to the contact region, distant points in both surfaces approach each other by an indentation ΔD $(=Dc-D)$ given by $\Delta D^3=(9/16)\pi^2(K_{mica+KS1})^2\Delta F^2/R$, where Dc represents the thickness of the S1 monolayer. This theory is satisfied as long as there is no deformation by the adhesion between the two contact surfaces. Indeed, in our experiments, deformation on the interference fringe was not observed because the adhesion forces were negligibly small. Thus our analysis is applicable by using the Hertz theory. For the interaction between the S1 monolayer and mica, using an approximation of E_{mica} $(\sim 90\ GPa) >> E_{S1}$, K_{mica} is negligibly small in comparison with K_{S1}. Accordingly, we approximately obtained the following equations: $r_0^3=(3/4)\pi K_{S1}R\Delta F$ and $\Delta D^3=(9/16)\pi^2 K_{S1}^2\Delta F^2/R$.

By using the above relationship between ΔF and ΔD, we analyzed Young's modulus of the S1 molecule. On the other hand, the stiffness of S1 is estimated in the following way. The true contact area S between mica and the S1 monolayer is given by πr_0^2. When s is defined as the occupied area of a single S1, the applied load per single S1, f, may be given by $\Delta F/(S/s)$. The density of S1 was determined by using the quartz crystal microbalance. If the proportional relation between the applied force f and the indentation ΔD is established, the slope in our experimental plot approximately corresponds to the stiffness, k, of a single S1.

Estimation of ATP release and sample damage by UV light

ATP was liberated from caged ATP by irradiating with UV light guided from a xenon lamp (HLS100UM, Hoya-Schott, Japan) (see Fig. 1). The intensity of the UV light on the specimen was about 5 mW. The effective UV-illuminated area was about 1 mm^2 in the vicinity of the contact area. The time course of ATP release was estimated by measuring the shortening velocities of myofibrils isolated from a rabbit glycerinated psoas muscle fiber.

We evaluated the UV damage to the specimen using myofibrils. The shortening of the velocities of myofibrils on UV exposure decreased linearly with an increase in the irradiation time [t (s)]. The decreasing curve against the relative velocity was fit well by $(100-0.057t)\%$ up to 20 min. The decrease during the first 20 s was only ~1%. Therefore, the damage to the recombinant S1 by the UV light during the 20 s of irradiation seemed to have been negligibly small for the enzymatic activity.

Results and discussion

The absorption density of S1 molecules on the Ni^{2+}-NTA-covered surface was estimated by using a quartz crystal microbalance. Figure 2 indicates the time course of absorption on the Ni^{2+}-NTA substrate after the

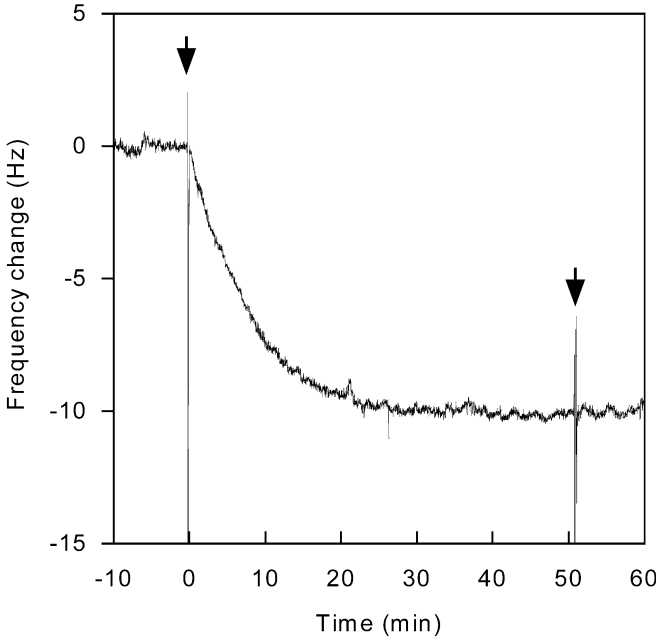

Fig. 2 Estimation of occupied area per S1 on the Ni^{2+}-NTA-covered surface. An S1 solution was injected to react covalently with Ni^{2+}-NTA at zero time, where we exchanged quickly a buffer solution immersed in a small chamber (~400 μL) for the S1 solution. Then, to stop the adsorbing reaction, we again exchanged the S1 solution for the buffer solution after about 50 min. *Arrows* denote the solution exchange. The data curve was fit well with $-10.2[\mathrm{Hz}]\{1-\exp(-0.125t[\mathrm{min}])\}$, $r^2=0.985$; temperature, 25.0 ± 0.1 °C

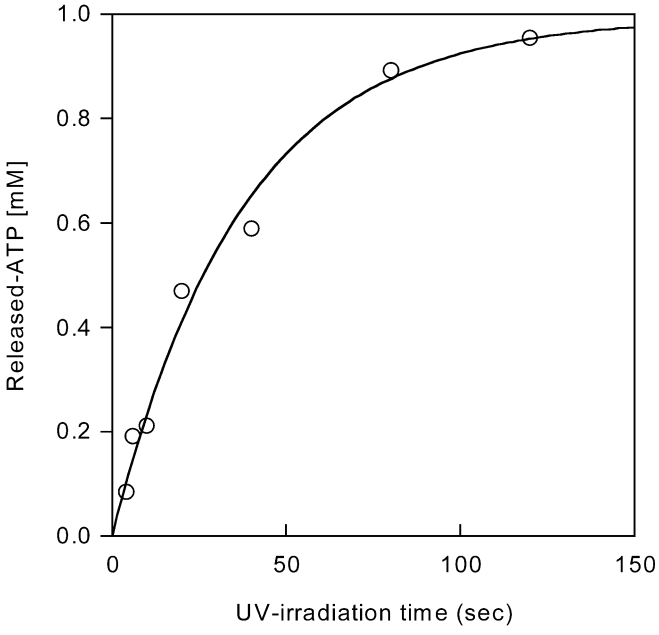

Fig. 3 The time course of ATP release initiated by UV irradiation. The time course of ATP release reached a plateau toward a maximum with a rate of 0.032 s^{-1} ($r^2=0.986$), which was estimated by measuring the shortening velocities of myofibrils isolated from a rabbit glycerinated psoas muscle fiber (data not shown). Here, in a plot of velocity versus ATP concentration, we obtained $V_{max}=3.5$ μm s^{-1}, $K_m=0.15$ mM

injection of an S1 solution. As molecules adsorb gradually on the electrode, the oscillation frequency of the Au electrode decreases in proportion to the adsorbed weight. To verify whether the S1 molecules were tightly fixed onto the substrate, we washed the surface with buffer solution. The frequency of the electrode hardly changed with the change of solutions. Thus S1 molecules seem to have been trapped tightly onto the Ni^{2+}-NTA substrate. The decreasing frequency curve was fit well with a single exponential. We obtained 160 ± 17 nm^2 (mean ± s.d., $n=3$) as the area occupied by the recombinant S1. On the other hand, we verified that S1 molecules did not attach on the NTA substrate without Ni^{2+} (data not shown).

We initiated ATP release by UV irradiation. Figure 3 shows the amount of released ATP as a function of UV irradiation time. The time course of ATP release reached exponentially a maximum plateau, which was estimated by measuring the shortening velocities of myofibrils isolated from a rabbit glycerinated psoas muscle fiber (data not shown). Here, in a plot of velocity versus ATP concentration, we obtained $V_{max}=3.5$ μm s^{-1}, $K_m=0.15$ mM. From Fig. 3 we can estimate that more than 0.4 mM ATP was released by the UV during 20 s. We chose 20 s as the period of UV irradiation. This duration was enough to obtain a moderate ATP concentration under as small UV damage as possible.

Figure 4A shows a typical force–distance profile between the two surfaces during the approaching process in a solution containing caged ATP. The upper surface was first brought toward the lower surface to measure the interaction force. The force (F) is normalized by the mean radius of curvature of the crossed cylinders ($R\approx1$ cm), which is plotted as a function of surface separation (D). Then F/R is related to the free energy per unit area between two flat surfaces, which is known as the Derjaguin approximation (Israelachvili 1992; Suda et al. 1999). When the two surfaces approached, the inward jump-in or attraction occurred at ~40 nm. We observed a long attractive force in this approach mode. Then, the repulsive force increased steeply, starting from ~17.5 nm, which corresponds to the free energy minimum, $\partial(F/R)/\partial D=0$. Each data point was manually taken in equilibrium (1–10 s). To capture as many recombinant S1 molecules ($>10^5$) as possible, we indented several nanometers more from this contact position.

After capturing S1 molecules between the two surfaces, the surfaces were gradually separated. From this separation process, the Young's modulus of the S1 molecules was calculated, based on the relationship between the applied force [$\Delta F=F(D)-F(D=17.5)$] and the displacement ($\Delta D=D-17.5$) (Lee and Belfort 1989; Suda et al. 1999), where the distance of 17.5 nm, which is close to the length dimension (16.5 nm) of the crystal structure of S1 (Rayment et al. 1993b), was used as the natural length of S1. In Fig. 4B, the data were fitted by using the relation of $\Delta F\propto\Delta D^{3/2}$, whose proportionality constant is related to the elasticity. A Young's modulus

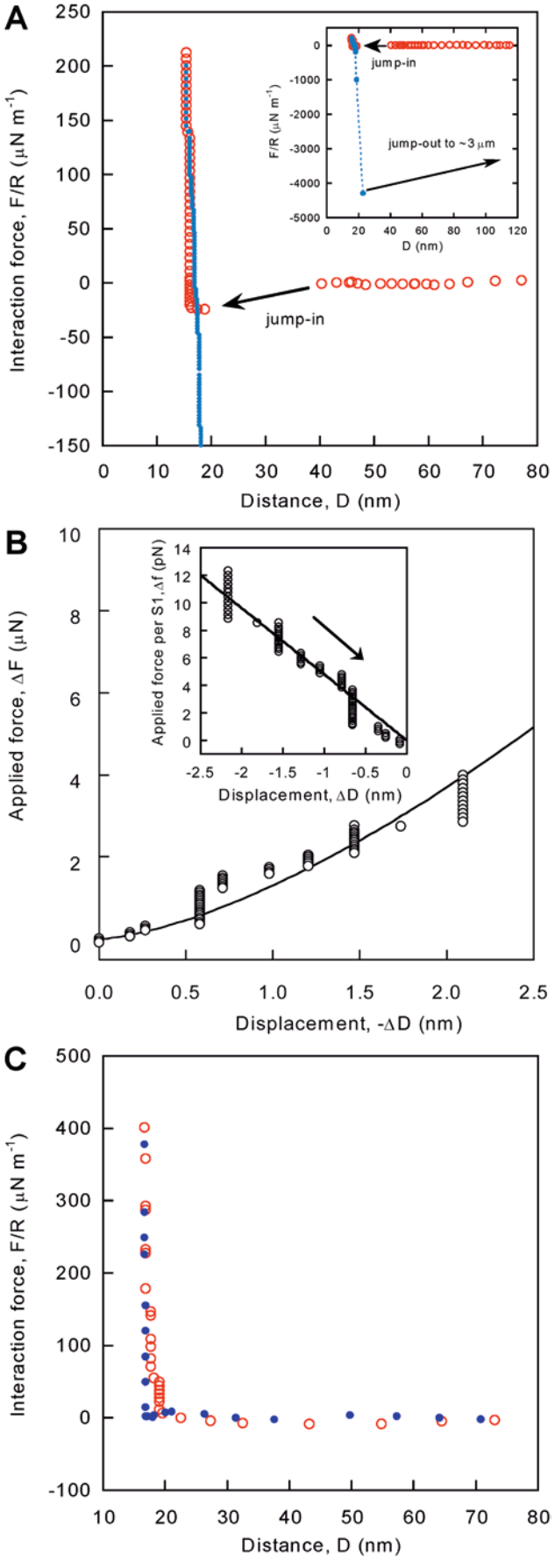

Fig. 4A–C Force measurements of myosin S1. **A** Force–distance profile for the interaction between the S1 monolayer and the maleimide-coated surfaces in a caged-ATP solution. The force axis (F) is normalized with respect to the radii of curvature (R) of the recombinant S1 monolayer and the maleimide-coated surfaces. The DTT reagent was independently injected at the point of maximum repulsive force before UV irradiation. *Red circles* and *filled blue circles* denote data in approach and separation modes, respectively. Stiffness of the double cantilever, 24.0 ± 1.1 N m^{-1}; R, 1.68 cm; captured number of the recombinant S1 molecules, 3.24×10^5. The *inset* shows the whole view of the force–distance profile. In this separation process we observed a large adhesion force. The two surfaces were separated by driving a DC motor with a fine control (a part of the *blue broken line* in the *inset*); the rupture force per S1 molecule to break the bond was ~300 pN at a loading rate of $\sim 10^2$ pN s^{-1}. **B** Young's modulus and stiffness (*inset*) of S1 in the case of **A**. By using the estimated Young's modulus, the applied forces were reduced to the forces per S1 molecule, Δf. The *continuous lines* were obtained by the least-squares method. See the text for more details. **C** Control experiment. The interaction force between the maleimide-covered surface and the S1 monolayer was measured in a solution including DTT from the beginning of the first approach mode. *Red circles* and *filled blue circles* denote data in approach and separation modes, respectively

of 0.67 GPa ($r^2 = 0.754$) was obtained using the nonlinear least-squares fitting, consistent with the value previously obtained (0.7 GPa) (Suda et al. 1999). The stiffness of S1 was also 4.80 pN nm^{-1} ($r^2 = 0.956$) from a stress–strain relationship per S1 molecule, as shown in the inset of Fig. 4B. The Young's modulus thus obtained was used to calculate the exact value of the contact area of two surfaces bridged with S1 molecules (~50 μm^2). The total number of S1 molecules in the contact area was then calculated from the S1 density determined earlier.

At the final stage of the separation process we observed a large adhesion force, as shown in the inset of Fig. 4A. We carried out a control experiment to determine whether the maleimide group of the opposite substrate was chemically bound with the fused SH group in the recombinant S1. Indeed, the large adhesion was remarkably reduced when the S1 monolayer contacted with the maleimide-covered surface at a condition in the presence of DTT from the beginning of the surface approach, as shown in Fig. 4C. This fact suggests that chemical bonds were formed between the SH and the maleimide groups.

At a near-zero load in the separation process (Fig. 4A), the sample was irradiated with UV for 20 s to release ATP molecules from the caged ATP solution (see Materials and methods). Figure 5A shows a typical example of the time course of displacement and force generated after the ATP release. Around 10 s after starting the UV irradiation, the distance between the two surfaces suddenly decreased, and then gradually increased toward the initial position. The experiments were repeated, and all data of the separation distance of the two surfaces at each time point were averaged as shown in Fig. 5B. When some amount of released ATP accumulated after the UV irradiation, the separation distance of the two surfaces quickly decreased, and it

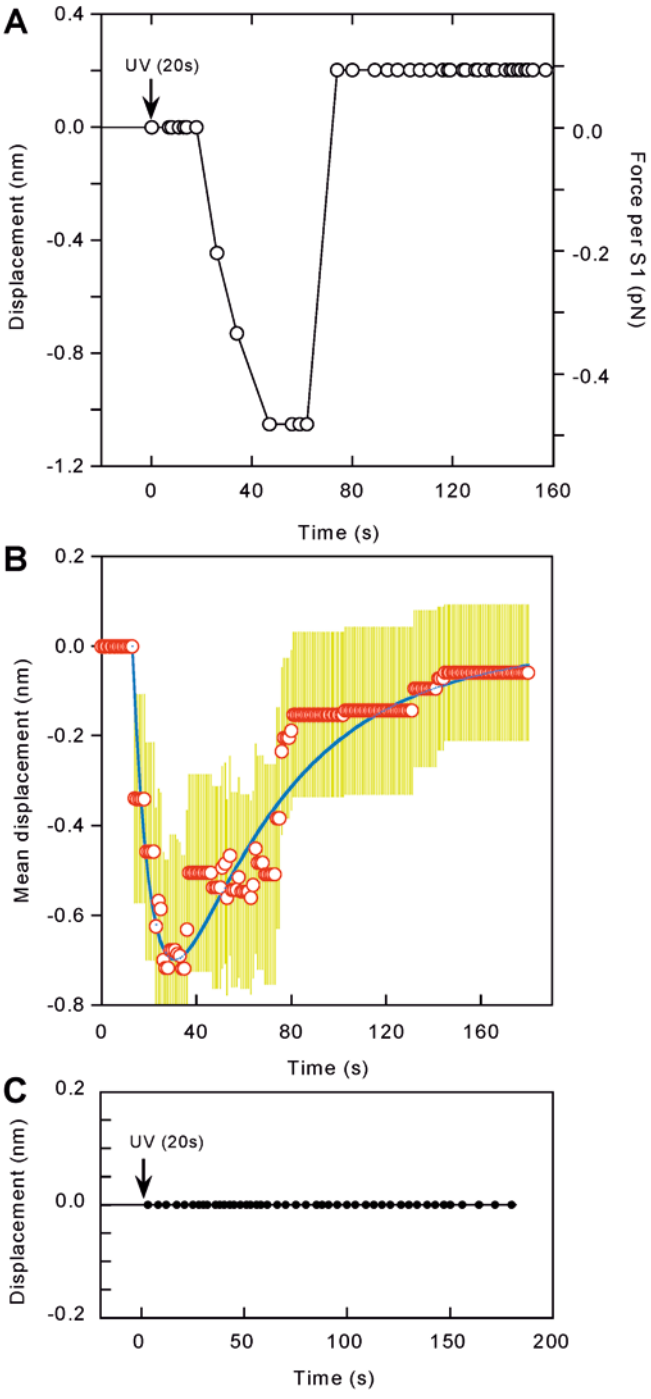

Fig. 5A–C The time courses of generation of displacement and forces by the recombinant S1 with ATP hydrolysis. **A** A typical record of the time courses of generation of displacements and forces by the S1 molecules. By using the estimated Young's modulus, the applied forces were reduced to the forces per the recombinant S1. The minus sign of displacement represents the shrinkage. **B** Time course of mean displacements by the recombinant S1 with ATP hydrolysis. Time zero denotes the starting point of UV irradiation during 20 s. *Red circles* denote the averaged data points for the experimental number of 17. *Continuous blue line*, a fitting curve. *Yellow lines*, standard errors included in each data point. **C** Control data. The same experiment in the caged ATP solution was carried out in the caged ADP solution. No change of displacement was observed within the limit of space resolution of the SFA. Temperature, 25 °C

gradually recovered toward the initial position. This time course of the recovery phase was best fit with a single exponential. The rate constant derived from the exponential curve was 0.02 s^{-1}. The first rapid decrease of the separation distance was well fit to a single exponential having a rate constant of 0.16 s^{-1}. When caged ADP was used in place of caged ATP, no distance change was observed, indicating that the observed distance changes in caged ATP upon the UV irradiation came from structural changes of the recombinant S1 induced by ATP hydrolysis. In fact, the rate of recovery of the separation distance (0.02 s^{-1}) was very similar to the steady-state rate of the P_i release of the recombinant S1 (0.04 s^{-1}) that was measured in this study. This result suggests that the recovery of the separation distance may correspond to the P_i-release process, i.e. the power stroke of the lever-arm. However, the rate of the first phase, the quick decrease of the separation distance, was much slower than that of the isomerization step of myosin ATPase cycle (17 s^{-1}) (Kuhlman and Bagshaw 1998), which seems to correspond to the recovery stroke of the lever-arm. The difference might be due to manually data record and the fact that ATP was released slowly by continuous UV irradiation and, therefore, the isomerization reaction of S1 molecules started in an uncoordinated way.

The force accompanying the distance change was detected with a double cantilever spring, as shown in Fig. 5A (also see Fig. 1 and Materials and methods). It must be noted here that the contact area varied from one experiment to another and, therefore, the total number of S1 molecules participating in this process varied as well. Thus, the force was averaged as that generated by single S1 molecules. The average values of force at the first rapid phase and the later slow phase were calculated to be 0.19 ± 0.04 pN/S1 (mean $\pm$ s.e.m., $n = 17$) and 0.23 ± 0.07 pN/S1, respectively. These values are close to ~0.1 pN generated by fusion myosin S1 (Itakura et al. 1993), which was measured by using a single actin filament bound to the tip of a glass micro-needle. However, it must be emphasized that they are the minimum values of force generated by the S1 molecule since we assume here that all the S1 molecules at the contact area contributed to the force generation. The physiological direction of myosin movement in cells is roughly in parallel to the long axis of a thick filament, whereas the direction of movement of the myosin head in our experimental system is roughly perpendicular to its long axis. Our detected structural change in the confined space between two surfaces is probably due to a twisting motion (Vale and Milligan 2000). On the other hand, the detected forces were measured under the force balance. Thus we do not need to take note of the direction of myosin movement because our aim was to detect force.

To exclude the possibility that expansion of the substrates with a local increase in the temperature as a

Table 1 Estimation of the displacement and the force generated by the recombinant S1[a]

Solution	Displacement (nm)		Force (pN)		Experiment number
	First change[b]	Recovery	First change[b]	Recovery	
Caged ATP	1.07 ± 0.12	1.05 ± 0.23	0.19 ± 0.04	0.23 ± 0.07	17
ATP free	≤ 0.10	≤ 0.10	≤ 0.01	≤ 0.01	10
Caged ADP	≤ 0.10	≤ 0.10	≤ 0.01	≤ 0.01	9

[a]The numerical values represent the mean ± s.d. The maximum values recorded for each experiment are averaged. All data were collected under a low load (< 0.1 pN). The estimated force gives the minimum (see the text for more details)
[b]These values denote the first distance change between two surfaces in the caged ATP solution after UV irradiation.

result of UV irradiation could cause the observed distance changes, control experiments were carried out in an ATP-free solution and in a solution containing caged ADP. Note that the optical method used here for measuring the surface separation actually measured the distance between the two silvered layers on the reverse sides of the mica sheets. It was verified that no error greater than 0.1 nm in the surface separation was caused by normal temperature variations (± 0.5 °C) under the present conditions. However, for temperature variations above ~1 °C, a correction to the composite mica sheets ($2T$) has to be made. The thermal expansion of mica is $\sim 10 \times 10^{-6}$ °C^{-1}; thus, for example, a 10 °C rise in the temperature of the liquid will expand the mica sheets by ~0.6 nm if $2T = 6$ μm. However, such a big change is unlikely because in these experiments the temperature change, by taking account of the photo energy of ~5 mW, the absorption of UV in the mica sheets (~4%), and the thermal conductivity (~1 W m^{-1} K^{-1}), is ~0.03 °C in a steady state. Indeed, no appreciable change in the separation distance was observed even when the UV was continuously irradiated for 5 min. The notion was further confirmed by the observation that the UV irradiation in a caged ADP solution did not cause any change in the separation distance within the limit (~0.1 nm) of the space resolution of the SFA, as shown in Fig. 5C and Table 1. Thus we could exactly exclude a possible artifact by the release of caged group.

Conclusions

Considering these results, it is suggested that the recombinant myosin S1 shrinks upon ATP binding and then recovers the initial conformation after the P_i release. Although the observed change in the separation distance (~1 nm) is less than the expected swing distance of the lever-arm swing (~5 nm), the discrepancy could be attributed to a lack of freedom of S1 molecules in the confined space or a particular orientation of the S1 molecules between the two surfaces. Both the shrinking and the recovery processes generated a force of at least ~0.2 pN/S1 molecule. This result implies that the S1 molecule has a capacity to generate force without the contribution of actin.

Acknowledgements We would like to express our thanks to Prof. K. Sutoh for his help and critical reading of the manuscript. We could not achieve this work without his contribution. We also thank M. Watanabe for his technical support with the ECR sputtering, and K. Kurihara, S. Aoki, T. Hagiwara, S. Yamada, and K. Ito for their assistance with the experiments. This work was supported by a Grant-in-Aid for Science Research on Priority Area (A) from the Ministry of Education, Science, Sports, and Culture of Japan.

References

Baker JE, Brust-Mascher I, Ramachandran S, LaConte LEW, Thomas DD (1998) A large and distinct rotation of the myosin light chain domain occurs upon muscle contraction. Proc Natl Acad Sci USA 95:2944–2949

Dobbie I, Linari M, Piassesi G, Reconditi M, Koubassova N, Ferenczi MA, Lombardi V, Irving M (1998) Elastic bending and active tilting of myosin heads during muscle contraction. Nature 396:383–387

Dominguez R, Freyzon Y, Trybus KM, Cohen C (1998) Crystal structure of a vertebrate smooth muscle myosin motor domain and its complex with the essential light chain: visualization of the prepower stroke state. Cell 94:559–571

Finer JT, Simmons RM, Spudich JA (1994) Single myosin molecule mechanics: piconewton forces and nanometre steps. Nature 368:113–119

Geeves MA, Holmes KC (1999) Structural mechanism of muscle contraction. Annu Rev Biochem 68:682–728

Hertz H (1881) J Reine Angew Math 92:156–171; (1896) Miscellaneous papers. Macmillan, London, p 146

Huxley AF (1957) Muscle structure and theories of contraction. Prog Biophys Biophys Chem 7:255–318

Huxley HE (1969) The mechanism of muscle contraction. Science 164:1356–1366

Irving M, Lombardi V, Piazzesi G, Ferenczi MA (1992) Myosin head movements are synchronous with the elementary force-generating process in muscle. Nature 357:156–158.

Irving M, Allen TStC, Sabido-David C, Craik JS, Brandmeier B, Kendrick-Jones J, Corrie JET, Trentham DR, Goldman YE (1995) Tilting of the light chain region of myosin during step length changes and active force generation in skeletal muscle. Nature 375:688–691.

Israelachvili J (1992) Intermolecular and surface forces, 2nd edn. Academic Press, London

Itakura S, Yamakawa H, Toyoshima YY, Ishijima A, Kojima T, Harada Y, Yanagida T, Wakabayashi T, Sutoh K (1993) Force-generating domain of myosin motor. Biochem Biophys Res Commun 196:154–150

Jeppesen C, Wong JY, Kuhl TL, Israelachvili JN, Mullah N, Zalipsky S, Marques CM (2001) Impact of polymer tether length on multiple ligand-receptor bond formation. Science 293:465–468

Kuhlman PA, Bagshaw CR (1998) ATPase kinetics of the *Dictyostelium discoideum* myosin II motor domain. J Muscle Res Cell Motil 19:491–504

Lee C-S, Belfort G (1989) Changing activity of ribonuclease A during adsorption: a molecular explanation. Proc Natl Acad Sci USA 86:8392–8396

Mangipudi VS (1995) Analysis and application of a 5-layer multiple beam interferometer in the surface forces apparatus. J Colloid Interface Sci 175:484–491

Rayment I, Rypniewski WR, Schmidt-Base K, Smith R, Tomchick DR, Benning MM, Winkelmann DA, Wesenberg G, Holden HM (1993a) Structure of the actin-myosin complex and its implications for muscle contraction. Science 261:58–65

Rayment I, Holden HM, Whittaker M, Yohn CB, Lorenz M, Holmes KC, Milligan RA (1993b) Three-dimensional structure of myosin subfragment-1: a molecular motor. Science 261:50–58

Sasaki N, Shimada T, Sutoh K (1998) Mutational analysis of the switch II loop of *Dictyostelium* myosin II. J Biol Chem 273:20334–20340

Sasaki YC, Suzuki Y, Yagi N, Adachi S, Ishibashi M, Suda H, Toyota K, Yanagihara M (2000) Tracking of individual nanocrystals using diffracted x-rays. Phys Rev E 62:3843–3847

Shih WM, Gryczynski Z, Lakowicz JR, Spudich JA (2000) A FRET-based sensor reveals large ATP hydrolysis-induced conformational changes and three distinct states of the molecular motor myosin. Cell 102:683–694

Suda H, Sasaki YC, Oishi N, Hiraoka N, Sutoh K (1999) Elasticity of mutant myosin subfragment-1 arranged on a functional silver surface. Biochem Biophys Res Commun 261:276–282

Suzuki Y, Yasunaga T, Ohkura R, Wakabayashi T, Sutoh K (1998) Swing of the lever arm of a myosin motor at the isomerization and phosphate-release steps. Nature 396:380–383

Vale RD, Milligan RA (2000) The way things move: looking under the hood of molecular motor proteins. Science 288:88–95

Wakabayashi K, Tokunaga M, Kohno I, Sugimoto Y, Hamanaka T, Takezawa Y, Wakabayashi T, Amemiya Y (1992) Small-angle synchrotron x-ray scattering reveals distinct shape changes of the myosin head during hydrolysis of ATP. Science 258:443–447

Yanagida T, Iwane AH (2000) A large step for myosin. Proc Natl Acad Sci USA 97:9357–9359